

# Time-dependent probability distribution functions for orientational motions of segments in polymer chains

Turkan Haliloglu, Burak Erman, and Ivet Bahar

*Polymer Research Center and School of Engineering, Bogazici University, Bebek 80815, Istanbul, Turkey*

(Received 20 April 1992; accepted 26 May 1992)

The spatial orientation of vectors rigidly embedded in polymer chains are described in terms of time-dependent joint probability distribution functions. Serial expansion in terms of double spherical harmonics is adopted for the probability distribution functions, with the coefficients therein evaluated from Brownian dynamics simulations. Truncation of the series after the second-order harmonics accurately reproduces the results of Brownian dynamics simulations for a 50 bond polyethylene chain whose ends are held fixed at various extensions.

## I. INTRODUCTION

The anisotropy of segmental dynamics in polymer chains has been investigated some years ago in terms of double spherical harmonics by Tao<sup>1</sup> and Jarry and Monnerie.<sup>2</sup> These authors formulated the time-dependent orientation distribution for vectors affixed to chains in a form suitable for the study of local chain dynamics by polarized fluorescence experiments. In recent years, interest has been refocused on the problem of the anisotropy of local static and dynamic orientational correlations following the developments in deuterium NMR spectroscopy.<sup>3</sup> The present paper tests the adequacy of spherical harmonics series expansion of the joint distribution function for chains with fixed ends at various extensions.

Oriental motions of segments depend sensitively on intramolecular and intermolecular configurational characteristics of the chains and are therefore of significant interest for the understanding of polymer behavior. In the preceding paper,<sup>4</sup> results of Brownian dynamics simulation were used to study the internal orientational dynamics of deformed polyethylene model chains as a function of their end-to-end separation. The rates of transitions between isomeric states and bond orientational autocorrelations and cross correlations were observed to be strongly affected by the perturbation of chain dimensions. Conformational correlation functions were evaluated therein for backbone bonds and the two autocorrelation functions,  $M_1(t)$  and  $M_2(t)$ , associated with the reorientation of bond vectors were analyzed. In the present paper, the analysis is extended to the study of local orientational motions in deformed chains as seen by a laboratory-fixed observer at a given orientation with respect to the chain vector. Time-dependent joint probability functions in the form of a double spherical harmonics series are developed for the orientation of bond vectors. The coefficients of this series are evaluated numerically for a polyethylene chain of 50 bonds using the results of the Brownian dynamics simulation described in detail in Ref. 4.

In Sec. II the serial expression for the time-dependent probability distribution function is given. In Sec. III the coefficients of this series are evaluated from simulations for chains of various extensions. The series are developed up to

the second-order terms in the spherical harmonics and the analytical expressions are compared with the results from Brownian dynamics simulations. Graphical analysis of the probability distribution functions in Sec. IV indicates the suitability of the closed form expressions for an effective description of local orientational dynamics of polymer chains.

## II. DISTRIBUTION FUNCTION FOR SEGMENTAL ORIENTATION

The  $z$  axis of the laboratory-fixed coordinate system is chosen along the direction of the end-to-end vector  $\mathbf{r}$ . The  $n$ th atom is kept fixed along the  $z$  axis. The zeroth atom of a 50 bond chain is located at the origin. The  $z$  axis chosen in this manner forms an axis of cylindrical symmetry about which all configurations of the chain are equally accessible. The orientational dynamics of a vector  $\mathbf{m}$ , shown in Fig. 1, is analyzed.  $\mathbf{m}$  is assumed to be rigidly affixed to a point along the chain. The axes shown in Fig. 1 are parallel to the respective axes of the laboratory-fixed coordinate system. The state of separation of the two ends of the chain is represented by the parameter  $\lambda$  defined as the ratio of the fixed end-to-end distance  $r$  to the root-mean-square distance of the end-to-end vector of the unperturbed chain. Four different values of extension ratios  $\lambda$  are considered in this study as shown in the third row of Table I.

The instantaneous orientation of  $\mathbf{m}$  may be described by spherical polar angles  $\psi = (\omega, \Psi)$ , where  $\omega$  is the angle between the  $z$  axis and  $\mathbf{m}$ , and  $\omega$  is the angle between the  $x$  axis and the projection of  $\mathbf{m}$  on the  $xy$  plane. The joint probability of orientation  $\Omega$  at time  $t$  and  $\Omega_0$  at time  $t_0$  for the vector  $\mathbf{m}$  is denoted as  $p_r(\Omega, t; \Omega_0, t_0)$  for a chain with end-to-end separation  $\mathbf{r}$ . This probability may be expressed in terms of a double spherical harmonics series as

$$p_r(\Omega, t; \Omega_0, t_0) = \sum_{k=0}^{\infty} \sum_{l=0}^{\infty} \sum_{m=-k}^k \sum_{n=-l}^l a_{kl}^{mn} Y_k^m(\Omega_0) Y_l^n(\Omega)^*, \quad (1)$$

where  $Y_k^m(\Omega_0)$  are the spherical harmonics given by<sup>5</sup>

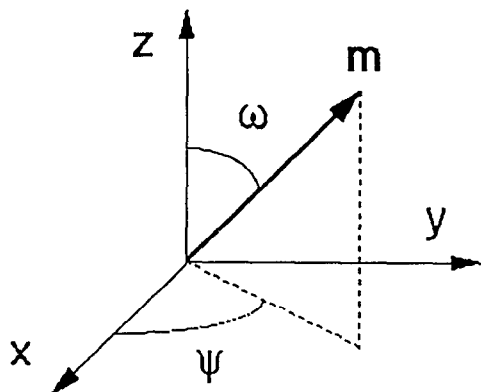


FIG. 1. Orientation of the vector  $\mathbf{m}$  with respect to the laboratory-fixed frame  $xyz$ , defined by the polar angle  $\omega$  and the azimuthal angle  $\psi$ .

$$Y_k^m(\Omega) = Y_k^m(\omega, \Psi) \\ = (-1)^m \left( \frac{(2k+1)(k-m)!}{4\pi(k+m)!} \right)^{1/2} P_k^m(\cos \omega) e^{im\Psi} \quad (2)$$

with  $P_k^m(\cos \omega)$  expressed in terms of the Legendre polynomial  $P_k(\cos \omega)$  of degree  $k$  as

$$P_k^m(\cos \omega) = (\sin^2 \omega) \frac{d^m}{dx^m} P_k(\cos \omega). \quad (3)$$

$P_k(\cos \omega)$  is equal to  $(\cos \omega)$  and  $(\frac{3}{2} \cos^2 \omega - \frac{1}{2})$  for  $k=1$  and 2, respectively. The asterisk in the superscript position in Eq. (1) denotes the complex conjugate and  $a_{kl}^{mn}$  is the coefficient obtained as

$$a_{kl}^{mn} = \langle Y_k^m(\Omega_0) Y_l^n(\Omega)^* \rangle_r \quad (4)$$

$$= \int_{\Omega} \int_{\Omega_0} p_r(\Omega, t; \Omega_0, t_0) Y_k^m(\Omega_0) Y_l^n(\Omega)^* d\Omega_0 d\Omega, \quad (5)$$

where  $d\Omega = \sin \omega d\omega d\Psi$  and  $d\Omega_0 = \sin \omega_0 d\omega_0 d\psi_0$  and the variable  $\omega$  and  $\psi$  vary in the ranges  $0 \leq \omega \leq \pi$  and  $0 \leq \psi \leq 2\pi$ . The angular brackets with the subscript  $r$  denote the time average over all possible configurations of the chain with fixed  $r$ .

We define the probability function  $p_r(\Omega, t; \Omega_0, t_0)$  in Eq. (1) as the probability obtained for a single chain with fixed  $r$  along the  $z$  axis. In adopting this definition, we pay attention to directivity along the chain by assuming that the two ends of the chain are distinguishable. We make this choice in the interest of interpreting our computer simulation results obtained for the single chain. This choice of averaging does not obtain, for example, in spectroscopic experiments where the two ends of chains are not distin-

guishable and odd powers of  $\cos \omega$  necessarily vanish when  $t=0$ . This point will be discussed in more detail later.

The following relations exist between the coefficients of Eq. (1) from cylindrical symmetry:

$$a_{kl}^{mn} = a_{kl}^{-m-n} = a_{kl}^m \delta_{mn} \quad (6)$$

where  $\delta_{mn}$  is the Kronecker delta. With these definitions, Eq. (1) may be written up to the second-order terms in the spherical harmonics as

$$p_r(\Omega, t; \Omega_0, t_0) = \frac{1}{16\pi^2} \left( 1 + \sum_{i=1}^9 \langle f_i \rangle_r f_i \right), \quad (7)$$

where the nine functions  $f_i$  are given as

$$\begin{aligned} f_1 &= (3/2)^{1/2} (\cos \omega + \cos \omega_0), \\ f_2 &= \frac{1}{2} (5/2)^{1/2} [(3 \cos^2 \omega_0 - 1) + (3 \cos^2 \omega - 1)], \\ f_3 &= \frac{1}{4} (30)^{1/2} [\cos \omega_0 (3 \cos^2 \omega - 1) \\ &\quad + \cos \omega (3 \cos^2 \omega_0 - 1)], \\ f_4 &= 3 \cos \omega_0 \cos \omega, \\ f_5 &= \frac{5}{4} (3 \cos^2 \omega_0 - 1) (3 \cos^2 \omega - 1), \\ f_6 &= \frac{3}{2} 2^{1/2} \sin \omega_0 \sin \omega \cos(\psi - \psi_0), \\ f_7 &= \frac{15}{2} 2^{1/2} \sin \omega_0 \cos \omega_0 \sin \omega \cos \omega \cos(\psi - \psi_0), \\ f_8 &= \frac{3}{2} (5)^{1/2} [\sin \omega_0 \cos \omega_0 \sin \omega \\ &\quad + \sin \omega \cos \omega \sin \omega_0] \cos(\psi - \psi_0), \\ f_9 &= \frac{45}{24} 2^{1/2} \sin^2 \omega_0 \sin^2 \omega \cos 2(\psi - \psi_0). \end{aligned} \quad (8)$$

The averages appearing in Eq. (7) are defined as

$$\langle f_i \rangle_r = \int_{\Omega} \int_{\Omega_0} f_i p_r(\Omega, t; \Omega_0, t_0) d\Omega_0 d\Omega. \quad (9)$$

For an ensemble of chains with indistinguishable ends for which the  $z$  axis may equally be directed from the  $n$ th atom to the zeroth atom, the averages  $\langle f_i \rangle_r$  containing odd powers of  $\cos \omega_0$  should reduce to zero, thus leaving the four averages  $\langle f_2 \rangle_r$ ,  $\langle f_5 \rangle_r$ ,  $\langle f_6 \rangle_r$ , and  $\langle f_9 \rangle_r$ . Evaluation of the functions  $\langle f_i \rangle_r$  completely describes the probability distribution function up to the second-order terms in the spherical harmonics.

### III. EVALUATION OF $\langle f_i \rangle_r$ FROM BROWNIAN DYNAMICS SIMULATION DATA

In this section, the averages  $\langle f_i \rangle_r$  are evaluated from trajectories of the vector  $\mathbf{m}$  over sufficiently long-time ranges by using the Brownian dynamics simulations of Ref. 4 for a polyethylene chain at four different degrees of extension  $\lambda$ . The vector  $\mathbf{m}$  is chosen in the present study as a unit vector along the backbone carbon-carbon bond. All calculations throughout the paper are based on the average behavior of the central 20 bond vectors of the chain. The total duration of the four simulations are shown in the second row of Table I. Time steps of 5 fs were used in simulations. The averages are calculated for the four runs

TABLE I. Simulation data.

Run	I	II	III	IV
$\lambda$	0.37	0.91	1.38	2.00
$t_f$ (ns)	16.5	18.0	17.0	18.0

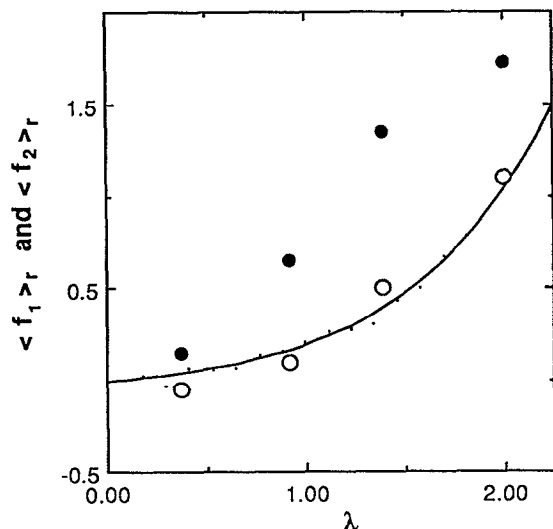


FIG. 2. Dependence of the coefficients  $\langle f_1 \rangle_r$  and  $\langle f_2 \rangle_r$  defined in Eqs. (8) and (9) on the extension ratio  $\lambda$ . The solid and open circles are computed for  $\langle f_1 \rangle_r$  and  $\langle f_2 \rangle_r$ , respectively, from Brownian dynamics simulations of 50-bond chains. The curve was obtained (Ref. 6) for  $\langle f_2 \rangle_r$  in a recent Monte Carlo study of orientation in deformed potential-energy chains.

by using Eq. (2). The first two averages,  $\langle f_1 \rangle_r$  and  $\langle f_2 \rangle_r$  are independent of time inasmuch as they depend only on the instantaneous values of  $\omega$  and the simulations are performed at steady-state conditions. Their dependence on the degree of extension are shown in Fig. 2. The solid circles in Fig. 2 represent the  $\langle f_1 \rangle_r$  values obtained from simulations. The open circles are for  $\langle f_2 \rangle_r$ . The solid line is obtained for  $\langle f_2 \rangle_r$  from a previous Monte Carlo study<sup>6</sup> of orientation in deformed polyethylene chains. The points and the curves indicate the good agreement between Brownian dynamics simulations and the Monte Carlo calculations. Small differences between the results of the two methods may be attributed to the fact that the bond orientational potentials were taken to be pairwise dependent in the Monte Carlo calculations while they are assumed to be independent in the present Brownian dynamics simulations. The curve as well as the open circles in Fig. 2 exhibit the dominant  $\lambda^2 - 1/\lambda$  behavior of the orientation function.

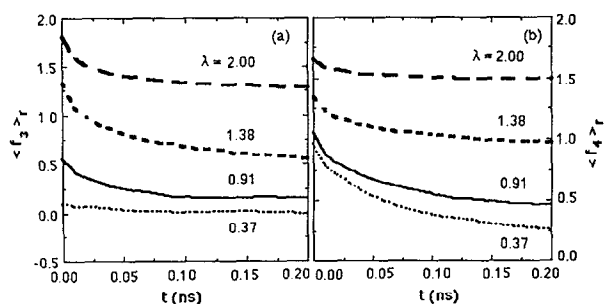


FIG. 3. Time decay of the coefficients (a)  $\langle f_3 \rangle_r$  and (b)  $\langle f_4 \rangle_r$ , defined in Eqs. (8) and (9), obtained from BD trajectories of deformed 50-bond chains with the indicated degrees of extension at 400 K.

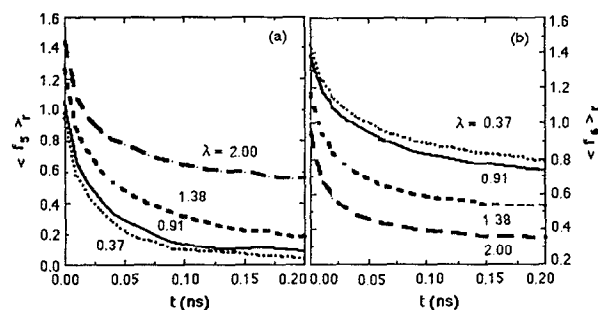


FIG. 4. Time decay of the coefficients (a)  $\langle f_5 \rangle_r$  and (b)  $\langle f_6 \rangle_r$ . See legend to Fig. 3.

The decay of the functions  $\langle f_3 \rangle_r$  and  $\langle f_4 \rangle_r$  with time are presented in Figs. 3(a) and 3(b), respectively, for the four different degrees of extension. In Fig. 3(a) the curves display different relaxational behavior at different degrees of extension. Strongest time dependence is observed for the intermediate extension of  $\lambda = 1.38$ . The highly compressed chain exhibits only a small amount of decay. The dependence of  $\langle f_4 \rangle_r$  on strain presented in Fig. 3(b) exhibits, on the other hand, a systematic pattern such that the highly stretched chain rapidly decays to its asymptotic value while both the magnitude and the rate of decay for the highly compressed chain are significant. The behavior of  $\langle f_5 \rangle_r$  and  $\langle f_6 \rangle_r$  are shown in Figs. 4(a) and 4(b), respectively. Both functions depend strongly on time and extension. For a given  $\lambda$ ,  $\langle f_5 \rangle_r$  asymptotically converges to the square of the corresponding  $\langle f_2 \rangle_r$  as dictated by the expressions given in Eq. (8). The decay curves for the functions  $\langle f_7 \rangle_r$  and  $\langle f_8 \rangle_r$  are displayed in Figs. 5(a) and 5(b). The values of  $\langle f_8 \rangle_r$  for  $\lambda = 1.38$  and 2.00 are very close to each other which is representative of a saturation effect at higher levels of stretching. Large reduction in the values of  $\langle f_8 \rangle_r$  upon compression to  $\lambda = 0.37$  should also be noted. Finally, the decay curves for  $\langle f_9 \rangle_r$  are given in Fig. 6. The strain dependence of these curves exhibits the same trend as that of  $\langle f_8 \rangle_r$ .

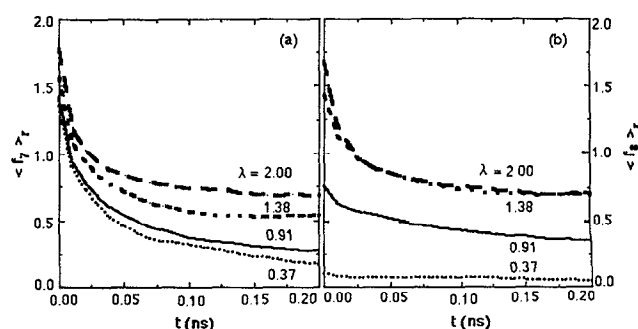


FIG. 5. Time decay of the coefficients (a)  $\langle f_7 \rangle_r$  and (b)  $\langle f_8 \rangle_r$ . See legend to Fig. 3.

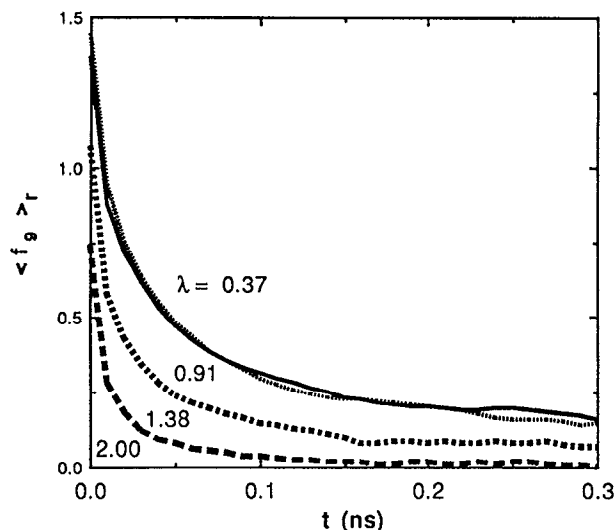


FIG. 6. Time decay of the coefficient  $\langle f_0 \rangle_r$ . See legend to Fig. 3.

#### IV. GRAPHICAL PRESENTATION OF THE DISTRIBUTION FUNCTIONS

In order to illustrate some features of the distribution functions, the surfaces generated from Eq. (7) for  $p_r(\Omega, t; \Omega_0, t_0)$  are plotted in Figs. 7 and 8 for vectors with specific initial orientation  $\Omega_0$  in chains of different extensions. The reorientational behavior of two major classes of vectors, namely those parallel and perpendicular to the direction of stretch are investigated in Figs. 7 and 8, respectively. Inasmuch as the conformational transitions in chains with fixed end-to-end separation conform with a stationary process, the elapsed time  $t-t_0$  rather than the two absolute times  $t_0$  and  $t$ , is of importance. The value  $t-t_0=0.5$  ns is considered in most of the calculations. This time is of the order of the relaxation time for the reorientational motions of  $\mathbf{m}$ . For economy of space, results for the two extreme cases of deformation,  $\lambda=0.37$  and  $\lambda=2.00$ , are displayed in parts (a) and (b) of Figs. 7 and 8.

In Figs. 7(a) and 7(b), the normalized probability surfaces for those vectors which were originally parallel to the  $z$  axis, i.e.,  $\omega_0=0^\circ$  are shown for the two extension ratios (a)  $\lambda=0.37$  and (b)  $\lambda=2.00$ , at  $t-t_0=0.5$  ns. The surface remains constant along the  $\psi$  axis, indicating that a vector originally along the  $z$  axis may result in any direction around the end-to-end vector with equal probability. This is a natural consequence of the cylindrical symmetry about the  $z$  axis. The dependence on  $\omega$ , on the other hand, may be observed from a given cross section of constant  $\psi$ . The stronger tendency of alignment along the stretch direction in the highly extended chain is clearly observable. The time evolution of a given probability surface may be seen from the comparison of Figs. 7(a) and 7(c), on the other hand, which are obtained for the respective time intervals  $t-t_0=0.5$  and 1.5 ns, for the compressed chain. With increasing time, the distribution of  $\omega$  approaches the equilibrium distribution of orientations with respect to the  $z$  axis which will be reconsidered later.

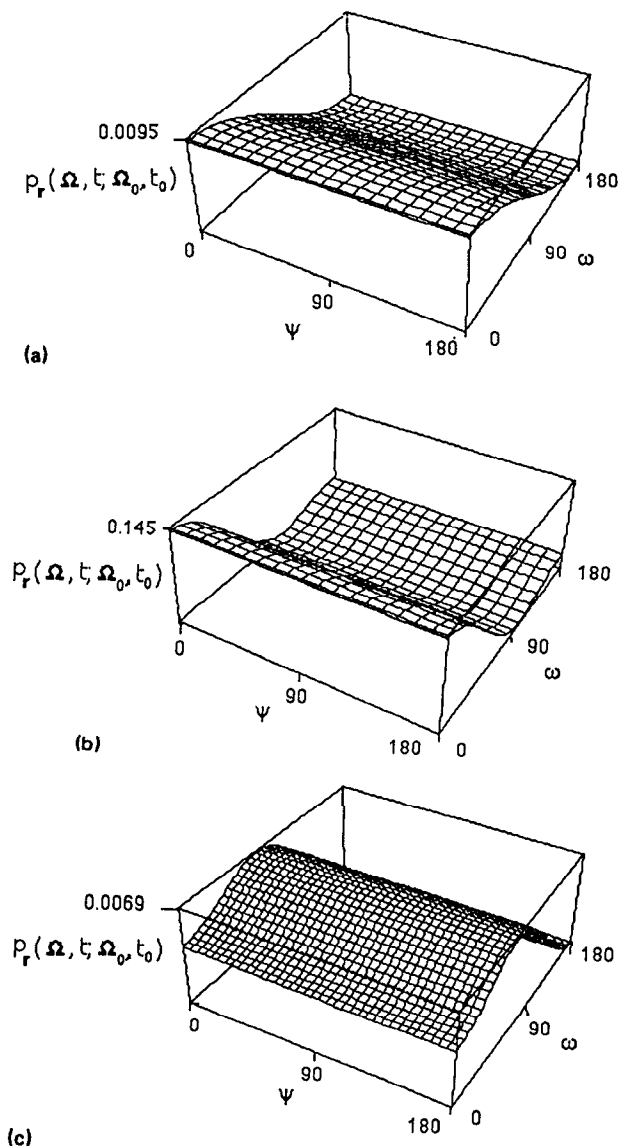
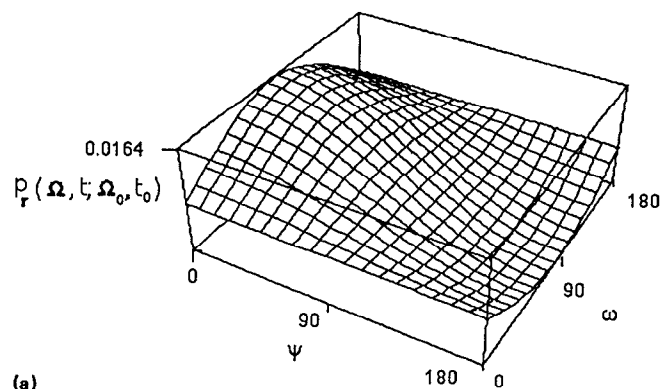
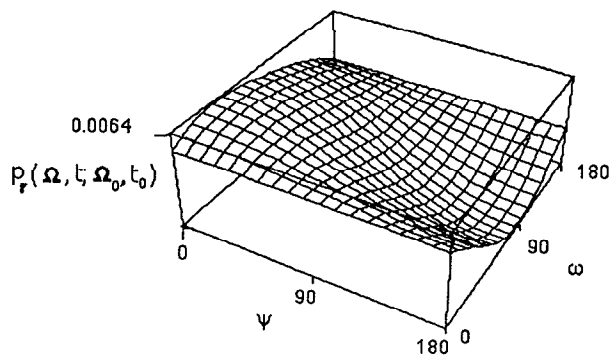


FIG. 7. (a) Time-dependent orientational probability distribution function  $p_r(\Omega, t; \Omega_0, t_0)$  as a function of  $\Omega = (\omega, \psi)$  calculated from Eq. (7) for bond vectors originally along the  $z$  axis ( $\omega_0=0^\circ$ ) in the chain subject to the extension ratio  $\lambda=0.37$  at  $t-t_0=0.5$  ns. (b) Probability surface  $p_r(\Omega, t; \Omega_0, t_0)$  for  $\omega_0=0^\circ$ ,  $t-t_0=0.5$  ns, and  $\lambda=2.00$ . (c) Probability surface  $p_r(\Omega, t; \Omega_0, t_0)$  for  $\omega_0=0^\circ$ ,  $t-t_0=1.5$  ns, and  $\lambda=0.37$ .

In Figs. 8(a) and 8(b), the probability surfaces calculated from Eq. (7) are shown for bond vectors which were originally perpendicular to the  $z$  axis and parallel to the  $x$  axis, i.e.,  $\omega_0=90^\circ$  and  $\psi_0=0^\circ$ . The extension ratios  $\lambda=0.37$  and 2.00 are considered in Figs. 8(a) and 8(b), respectively, with the same time interval of 0.5 ns. The general sloping down of the surface as  $\psi$  increases from  $0^\circ$  to  $180^\circ$  indicates that the vectors  $\mathbf{m}$  did not have sufficient time to spread out in the  $xy$  plane during the time interval of 0.5 ns. The higher ordinate value observed in Fig. 8(b) is again indicative of the enhanced tendency of the vectors perpendicular to the stretch direction in the highly extended chain, to escape their original orientation and to align along the preferred directions  $\omega=0^\circ$  and  $180^\circ$ . It is noted that the sense  $0^\circ$  is preferred rather than  $180^\circ$ . This is due to the fact that the two senses  $\pm \mathbf{r}$  of the end-to-end



(a)



(b)

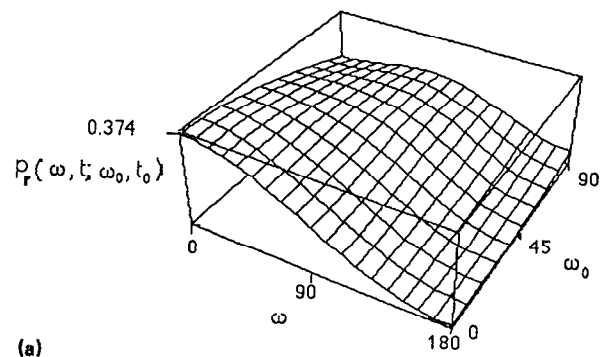
FIG. 8. (a) Probability surface  $p_r(\Omega, t; \Omega_0, t_0)$  as a function of  $\Omega = (\omega, \psi)$  calculated for bond vectors originally perpendicular to the  $z$  axis in the compressed chain.  $\Omega_0 = (\omega_0, \psi_0) = (90^\circ, 0^\circ)$ ,  $\lambda = 0.37$ , and  $t - t_0 = 0.5$  ns. (b) Probability surface  $p_r(\Omega, t; \Omega_0, t_0)$  for  $(\omega_0, \psi_0) = (90^\circ, 0^\circ)$ ,  $t - t_0 = 0.5$  ns, and  $\lambda = 2.0$ .

vector are *distinguishable* for the presently investigated bond vectors. Bond vectors exhibit a higher tendency to be oriented along  $+r$  sense, unless the chain is infinitely long.

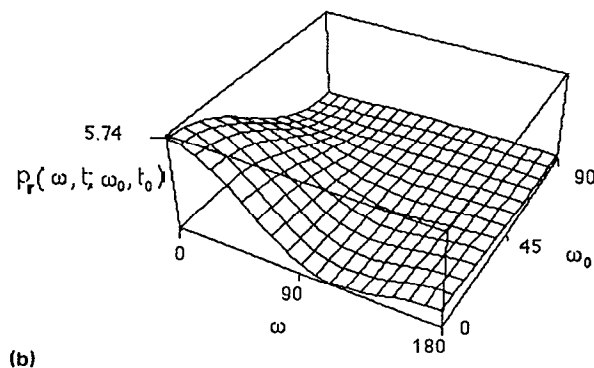
In Figs. 9(a)–9(c), the dependence of the probability surface on the polar angles  $\omega_0$  and  $\omega$  of  $\mathbf{m}$ , irrespective of the azimuthal angles  $\psi_0$  and  $\psi$ , are shown. The resulting surfaces represent the probability  $p_r(\omega, t; \omega_0, t_0)$  of the time-delayed joint event  $(\omega, t; \omega_0, t_0)$ . Summation over the azimuthal angles corresponds to integration of Eq. (7) with respect to these two variables. Performing the integrations leads to the joint probability,  $p_r(\omega, t; \omega_0, t_0)$  of the polar angles of  $\mathbf{m}$  as

$$p_r(\omega, t; \omega_0, t_0) = \frac{1}{4} \left( 1 + \sum_{i=1}^5 \langle f_i \rangle_r f_i \right). \quad (10)$$

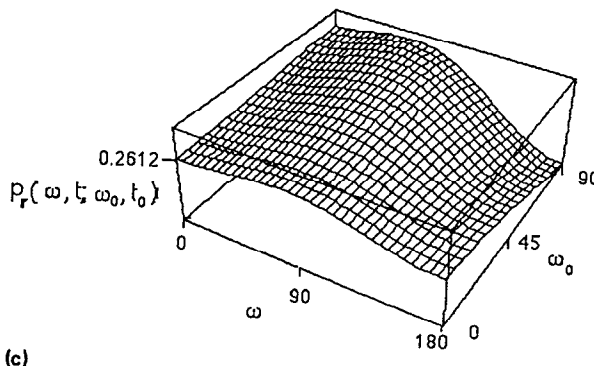
The surface is obtained by summing all occurrences of  $\mathbf{m}$  over the full range of azimuthal angles,  $0^\circ \leq \psi_0 < 360^\circ$  and  $0^\circ \leq \psi < 360^\circ$ , for  $t - t_0 = 0.5$  ns in Figs. 9(a) and 9(b), and for  $t - t_0 = 1.5$  ns in Fig. 9(c). Comparison of Figs. 9(a) and 9(b) obtained for  $\lambda = 0.37$  and 2.00, respectively, reveals the pronounced effect of chain extension on the time-delayed joint probability of polar angles. The relatively diffuse distribution of polar angles in the compressed chain is strongly sharpened and biased towards low values of  $(\omega, \omega_0)$  with increasing extension, as expected. Comparison of Figs. 9(a) and 9(c), on the other hand, displays the time evolution of the same probability surface obtained for



(a)



(b)



(c)

FIG. 9. (a) Dependence of the probability distribution function  $p_r(\omega, t; \omega_0, t_0)$  given by Eq. (9) on the polar angles  $\omega_0$  and  $\omega$ , for bond vectors in the highly compressed chain with  $\lambda = 0.37$  at the time interval  $t - t_0 = 0.5$  ns. (b) Probability surface  $p_r(\omega, t; \omega_0, t_0)$  for  $t - t_0 = 0.5$  ns and  $\lambda = 2.0$ . (c) Probability surface  $p_r(\omega, t; \omega_0, t_0)$  for  $t - t_0 = 1.5$  ns and  $\lambda = 0.37$ .

$\lambda = 0.37$ . The probability distribution obtained at long times in Fig. 9(c) indicates that the equilibrium state  $(\omega, \omega_0) = (90^\circ, 90^\circ)$  corresponding to transverse orientations of bond vectors with respect to the  $z$  axis is relatively favored in the case of compressed chains. One may better visualize the distributions by considering the intersections of the surface by planes perpendicular to the  $\omega_0$  axis. The curves obtained in this manner show the probability of occurrence of the final orientation  $\omega$  for a vector  $\mathbf{m}$  which was initially at  $\omega_0$ . Thus, the plane at  $\omega_0 = 0^\circ$  in Fig. 9(c) shows that bonds which were originally along the direction of the end-to-end vector  $\mathbf{r}$  will acquire a broad distribution of orientations after 1.5 ns. Similarly, the plane at  $\omega_0 = 90^\circ$  shows that bonds which were originally perpendicular to  $\mathbf{r}$  will orient more along the direction of  $\mathbf{r}$  and much less in

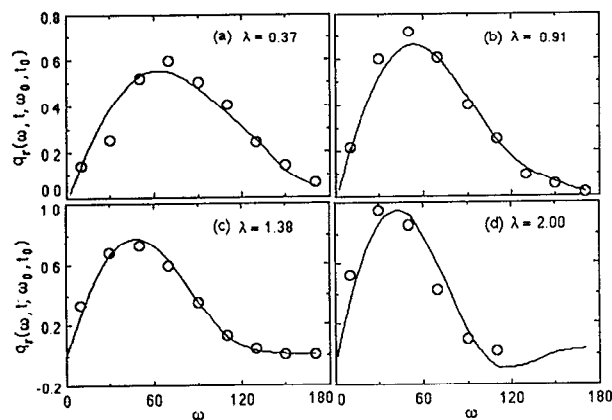


FIG. 10. Time-dependent conditional probability  $q_r(\omega, t; \omega_0, t_0)$  of occurrence of the polar angle  $\omega$  at the end of  $t-t_0=0.5$  ns for bond vectors originally along  $\mathbf{r}$ , in chains with different degrees of extension. The open circles are the results from BD trajectories and the curves are calculated using Eqs. (10) and (11),

the direction of  $-\mathbf{r}$ , in agreement with the implications of Fig. 8(b) discussed earlier.

## V. COMPARISON BETWEEN NUMERICAL AND ANALYTICAL RESULTS

The curves shown in Fig. 10 are obtained from Eq. (10) for the four values of  $\lambda$  and the time interval  $t-t_0=0.5$  ns. The ordinate values represent the conditional probabilities  $q_r(\omega, t; \omega_0, t_0)$  which are defined as

$$q_r(\omega, t; \omega_0, t_0) \equiv p_r(\omega, t; \omega_0, t_0) \sin \omega \Big/ \int_0^\pi p_r(\omega, t; \omega_0, t_0) \sin \omega d\omega$$

$$= \frac{p_r(\omega, t; \omega_0, t_0) \sin \omega}{p_r(\omega_0, t_0)}, \quad (11)$$

where  $q_r(\omega, t; \omega_0, t_0)$  gives the probability of occurrence of the orientation  $\omega$  at time  $t$ , given that the studied vector makes initially an angle  $\omega_0$  with the direction of extension. Thus, the surface represents the time-delayed normalized distribution of polar angles for those bonds which were originally along  $\mathbf{r}$ . The points are the results from Brownian dynamics simulations, obtained from direct counting of the joint event  $(\omega_0 \pm \Delta\omega_0, t_0; \omega \pm \Delta\omega, t)$ , with  $t-t_0=0.5$  ns and  $\omega_0=0^\circ$ . In order to have a sufficiently large population, the intervals in the counting process were taken as  $\Delta\omega_0 = \Delta\omega = 10^\circ$ . The agreement between the simulation results and the analytical expression is remarkable although the latter is truncated after the second-order terms. Negative values of the probability in part (d) of Fig. 10 indicate that the second-order approximation becomes insufficient as the degree of stretching becomes large. As expected, the curves become more sharply peaked and their maxima shift to smaller values of  $\omega$  upon stretching. However, the shift is relatively small and moves from about  $60^\circ$  for  $\lambda=0.37$  to  $40^\circ$  for  $\lambda=2.00$ .

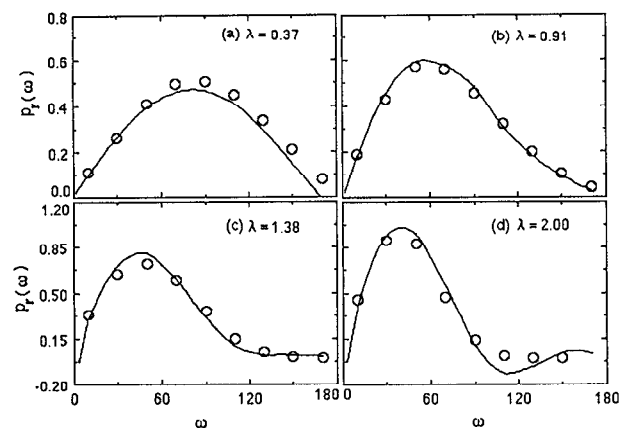


FIG. 11. Normalized equilibrium probability distribution function  $p_r(\omega)$  of the polar angle  $\omega$  in chains with different degrees of extension. The open circles are the results from BD trajectories and the curves are calculated from Eq. (12).

Further integration of Eq. (10) over the polar angle  $\omega_0$  after multiplying by  $\sin \omega_0$  results in the equilibrium probability distribution  $p_r(\omega)$  of the polar directions as

$$p_r(\omega) = \frac{1}{2} [1 + 3 \langle \cos \omega \rangle \cos \omega + \frac{5}{4} (3 \langle \cos^2 \omega \rangle - 1) \times (3 \cos^2 \omega - 1)]. \quad (12)$$

This quantity represents the equilibrium distribution of bond orientations with respect to the end-to-end vector  $\mathbf{r}$ , inasmuch as  $\mathbf{r}$  coincides with the  $z$  axis. Predictions of Eq. (12) are compared in Fig. 11 with results of Brownian dynamics simulations for the four different degrees of stretching. The good agreement between the numerical and analytical results confirms once again the suitability of the second-order expansion of time-dependent distribution functions in terms of spherical harmonics for an effective description of local orientational behavior of the chain.<sup>7</sup>

## VI. CONCLUSIONS

Series expansions has been widely used in chain statistics for representing the probability distribution functions associated with the equilibrium conformational properties of polymer chains. A common example is the Hermite polynomials series employed for the distribution of the end-to-end separation vector  $\mathbf{r}$ . Monte Carlo chain generation technique is conveniently used to determine the moments which appear in the coefficients of these series expansions. In analogy to this common procedure of equilibrium statistics, a series expansion is proposed in the present work for the time-dependent joint probability distribution of spatial orientations of vectorial quantities rigidly embedded in polymer chains. The Brownian dynamics simulation method is used in this case instead of Monte Carlo technique for the estimation of the time-dependent averages appearing in the coefficients of a spherical harmonics series. Comparison of the predictions of the series with the results from Brownian dynamics simulations confirms that the truncated series expansion may be safely employed for a quantitative analysis of local orientational

dynamics in deformed chains. Brownian dynamics simulation rests on the assumption of a Markoff process. The present calculations show that this Markoff process may accurately be described by a second-order series in spherical harmonics.

Present calculations were performed for deformed chains of 50 bonds. The analysis demonstrates that truncation of the series after the second-order spherical harmonics is suitable for an accurate description of the local orientational dynamics in those chains. For longer chains subject to weak deformation, the chain segments enjoy a higher degree of flexibility and, on a local scale, the orientation behavior of bond vectors approaches an unbiased distribution. As a result, the coefficients with odd-powered averages in the series will be vanishingly small and only the contributions from the remaining terms will survive, leading to much simpler expressions.

The description of local orientational dynamics by a closed form expression for time-delayed joint probability function allows for the prediction of the dynamic behavior of specific vectors observed in various experimental techniques. Examples are C-H bond vectors in NMR relaxation, transition moment vectors in fluorescence polarization, dipole moments in dielectric relaxation, etc. For the application of the presently developed probability distribution formalism to those specific vectorial quantities, it is sufficient to know the spatial orientation of those vectors with respect to the chain vector. Thus, the use of analytical expressions for time-dependent orientational distribution

functions may avoid repetitive simulations and may be particularly useful as a substitute for extensive computational analysis.

Inasmuch as the coefficients in the series are evaluated in a semiempirical way, based on BD trajectories, it should be noted that the expressions for the time-dependent distribution functions suffer from the same limitations as those inherently present in the simulation techniques. Absence of intramolecular effects such as bond rotational interdependence and volume exclusion, and neglect of intermolecular contributions such as specific solvent effects and hydrodynamic interactions are the main assumptions present in the BD simulations which are readily reflected upon the distribution functions.

#### ACKNOWLEDGMENT

Partial support by the Research Fund of Bogazici University, Grant No. 91P0029 is gratefully acknowledged.

<sup>1</sup>T. Tao, *Bipolymers* **8**, 609 (1969).

<sup>2</sup>J. P. Jarry and L. Monnerie, *J. Polym. Sci. Polym. Phys. Ed.* **16**, 443 (1978).

<sup>3</sup>H. W. Spiess, *Adv. Polym. Sci.* **66**, 23 (1985).

<sup>4</sup>T. Haliloglu, I. Bahar, and B. Erman, preceding paper, *J. Chem. Phys.* **97**, 4428 (1992).

<sup>5</sup>G. Arfken, *Mathematical Methods for Physicists* (Academic, San Diego, 1985), p. 680.

<sup>6</sup>B. Erman, T. Haliloglu, I. Bahar, and J. E. Mark, *Macromolecules* **24**, 901 (1991).

<sup>7</sup>M. E. Rose, *Elementary Theory of Angular Momentum* (Wiley, New York, 1957).